Journal of the Physical Society of Japan
Vol. 65, No. 11, November, 1996, pp. 3604-3614

Charge Excitations in Doped Mott Insulator in One Dimension

Michiyasu MORI and Hidetoshi FUKUYAMA

Department of Physics, the University of Tokyo, 7-3-1 Hongo, Bunkyo-ku, Tokyo 113

(Received July 4, 1996)

The doped Mott insulator in one dimension has been studied based on the phase Hamiltonian with the Umklapp scattering process, in which the charge degree of freedom is described by the quantum sine-Gordon model. The well-known equivalence between the quantum sine-Gordon model and the massive Thirring model for the spinless fermion makes it clear that the Mott-Hubbard gap originates from the Umklapp scattering process as was indicated by Emery and Giamarchi. Compressibility, density-density correlation function, frequency dependence of optical conductivity and Drude weight have been calculated in the presence of the impurity scattering treated in the self-consistent Born approximation. It is seen that there exists a crossover behavior in the spectral weight of charge excitations: the acoustic mode is dominant in small wave number region while the optical excitations across the Mott-Hubbard gap lie in large wave number region and that this crossover wave number is reduced as the Mott transition is approached.

KEYWORDS: Mott transition, Umklapp scattering process, quantum sine-Gordon model, massive Thirring model, compressibility, Drude weight, optical conductivity, impurity scattering

§1. Introduction

The Mott transition had so far been generally studied as metal-insulator transition which is caused by changing the strength of interaction (or the band width)[1,2] at a particular carrier density of half-filling. Since the discovery of high-T_c material, however, the behavior as the band filling (or doping rate) is varied in the vicinity of Mott insulator is the central issue, i.e., doping into the Mott insulator (doped Mott insulator). The high-T_c superconductivities can be considered as one of ground states of this doped Mott insulator. In the metallic state of this doped Mott insulator, anomalous behaviors are observed in transport and magnetic properties and then this state is called anomalous metallic state. The origin of those anomalies are considered to arise from characteristic nature of electronic states near the Mott transition.

For theoretical studies on this anomalous metallic phase, the Hubbard model has been frequently used. Although this model is considered to be the simplest Hamiltonian containing the essence of Mott transition, little is known about electronic properties near the transition as the doping rate is varied. In one dimension, the Hubbard model has been solved exactly by use of Bethe Ansatz[3] and anomalous behaviors of various quantities, compressibility, Drude weight etc., have been disclosed.[4,5] Further development has been achieved recently by the conformal field theory and asymptotic form of correlation functions have been determined.[6-8] These correlation functions behave as the power law which is characteristic to the Tomonaga-Luttinger liquid[9,10] where there exist excitations of acoustic modes both for charge and spin degrees of freedom in the limit of long wavelength. However, the detailed nature of the excitation spectrum has not been explored with this framework.

On the other hand, these properties can be explored by the bosonization.[11-13] The system far away from half-filling is in the Tomonaga-Luttinger regime.[9,10] As for a Mott insulator, i.e., at half-filling, Emery has shown that the Mott-Hubbard gap is seen to result from the Umklapp scattering process which is neglected in the Tomonaga-Luttinger regime.[14,15] The Mott transition caused by carrier doping, i.e., the doped Mott insulator, has been studied by Giamarchi.[16] In this study, optical conductivity was calculated within the second order of Umklapp scattering process by use of memory-function approximation and renormalization group method.[16-18] The Drude weight and its critical behavior toward the Mott transition has been investigated by Giamarchi[16] and Emery.[19] These studies on the optical conductivity are concerned with charge excitation at $q = 0$. On the other hand, charge excitation for finite q and ω near the Mott transition has been disclosed in our previous work[20] where we have found interesting features of spectral weight of charge excitations; i.e., the crossover behavior where the acoustic mode, which is the property of Tomonaga-Luttinger liquid, has a large spectral weight in the region of the small wave numbers while the optical mode, which originates from the inter-band excitation across the Mott-Hubbard gap, is weighted in the region of large wave numbers. The characteristic wave number of this crossover is reduced to zero as the metallic state merges to the insulating state.

In this present work, we will study in detail effects of disorder on charge excitations in the doped Mott insulator. To investigate such effects, the phase Hamiltonian[11-13] has been employed, where the charge degree of freedom is described by the quantum sine-Gordon model (QSG model) with misfit parameter representing the proximity to the half-filling.[11-14] The phase Hamiltonian has been originally derived by the bosonization to describe the low energy excitations for correlated sys-

tems in the limit of weak coupling[21,22] and has been considered to be qualitatively applicable to the regime of strong coupling by choosing properly the constants of the Hamiltonian.[23,24] In the classical treatment of this model, it is known that discommensuration lattice (soliton lattice), which will be identified with particles corresponding to the charge degree of freedom,[15] is created as the misfit parameter is varied and that there exists a transition between the commensurate and incommensurate phase as clarified by McMillan.[25]

We will study quantum mechanically the spectra of charge excitation by mapping QSG model onto the massive Thirring model (MT model).[26-30] This useful mapping was originally applied by Luther and Emery to the study of spin dynamics in 1D electron systems with backward scattering process[31,32] and later to the Mott transition[15-20] as mentioned above. However, the detailed study of charge excitation including disorder has not been carried out especially for the case where the Mott transition is approached by the carrier doping. By making use of the mapping and including disorder in terms of spinless Fermion, we will study the compressibility, density-density correlation function and optical conductivity in the presence of impurity scattering.

The structure of this paper is as follows. To make this paper complete, we summarize the results of some previous works by Emery, Giamarchi and ourselves in §2 and §3. In §2, we introduce the massive Thirring model to describe the charge degree of freedom. This model is derived from the phase Hamiltonian by using the bosonization. In §3, the charge excitation spectrum and optical conductivity are calculated in a clean system. In §4, we introduce an impurity scattering to investigate these quantities in disordered systems. §5 is for conclusion and discussion. We confine ourselves to absolute zero temperature in this paper.

§2. Hamiltonian and One Particle Properties

2.1 Phase Hamiltonian and classical picture of excitations

In one dimensional electron system, the low energy excitation of charge and spin degrees of freedom are independent of each another (spin-charge separation). Therefore, the phase Hamiltonian comprises two parts as follows;

$$H_\rho = \int \mathrm{d}x \left[A_\rho(\nabla\theta(x))^2 + B_\rho \cos(2\theta(x) - q_0 x) + C_\rho P(x)^2\right], \tag{2.1}$$

$$H_\sigma = \int \mathrm{d}x \left[A_\sigma(\nabla\phi(x))^2 + B_\sigma \cos(2\phi(x)) + C_\sigma M(x)^2\right], \tag{2.2}$$

where

$$[\theta(x), P(y)] = \mathrm{i}\delta(x-y), \tag{2.3}$$

$$[\phi(x), M(y)] = \mathrm{i}\delta(x-y). \tag{2.4}$$

$\theta(x)$ and $\phi(x)$ describe the fluctuation of charge and spin degree of freedom, respectively. The parameters A_ρ, B_ρ, C_ρ, A_σ, B_σ and C_σ depend on the coupling constants and the filling of band. The charge excitations, which are our main interest in this paper, are described by H_ρ, eq. (2.1), where the B_ρ-term is due to Umklapp scattering with $q_0 = G - 4k_0$, the misfit parameter. Here, G is the reciprocal lattice vector and $k_0 = \mu/v_{F0}$, with μ and v_{F0} being the chemical potential and the Fermi velocity of the noninteracting electrons, respectively. In the case of the noninteracting system, k_0 is the Fermi momentum. This misfit parameter controls the doping rate, i.e., the number of hole.

In order to understand the physical implication of QSG model, eq. (2.1), as a function of the misfit parameter, we first analyze the model semi-classically by assuming that the field operator, $\theta(x)$, consists of classical solution, $\theta_c(x)$, and fluctuation around this solution, $\hat{\theta}(x,t)$, as $\theta(x) = \theta_c(x) + \hat{\theta}(x,t)$. Here $\theta_c(x)$ and $\hat{\theta}(x,t)$ satisfy the following equations, respectively,

$$A_\rho(\nabla\theta_c(x))^2 + B_\rho\cos(2\theta_c(x)) = D, \tag{2.5}$$

$$\nabla^2\varphi(x) + \left[(m^2+\tilde{\omega}^2) - 2m^2\mathrm{sn}^2(mx/k;k)\right]\varphi(x) = 0, \tag{2.6}$$

where we assume $\hat{\theta}(x,t) = \varphi(x)\mathrm{e}^{\mathrm{i}\omega t}$ and

$$m^2 = \frac{2B_\rho}{A_\rho},$$

$$k^2 = \frac{2m^2}{m^2 + 2D/A_\rho},$$

$$\tilde{\omega}^2 = \frac{\omega^2}{4A_\rho C_\rho}. \tag{2.7}$$

In eq. (2.6), $\mathrm{sn}^2(mx/k;k)$ is the Jacobian elliptic function with the parameter k. An integral constant, D, is to be evaluated by the solution, $\theta_c(x)$, which minimizes the energy per unit length, ϵ, given by,

$$\epsilon = \frac{1}{2\pi l}\int_0^{2\pi l} \mathrm{d}x A_\rho(\nabla\theta_c(x) + q_0)^2 + B_\rho\cos(2\theta_c(x)), \tag{2.8}$$

where l is defined as, $2\pi l = (2k/m)K(k)$, and identified to a mean distance between discommensuration (DC)s. $K(k)$ is the first kind complete elliptic integral with parameter k. In the classical solution, $\theta_c(x) = \pi/2 - \mathrm{sn}(mx/k;k)$, there exist a transition between the commensurate (C) and incommensurate (IC) phase as is shown in Fig. 1 for $m = 1$ and some choices of k.[25] Since the fluctuation of number density of charge, $n(x)$, in the long wave length limit ($q \ll 2k_0$) is,

$$n(x) \sim \frac{\nabla\theta(x)}{\pi}, \tag{2.9}$$

the DCs of $\theta_c(x)$ are identified as particles.[15] Thus the commensurate (incommensurate) phase can be considered to be an undoped (doped) state. In the IC phase near the Mott transition, the DC lattice is created and its excitation spectrum, which is the eigenvalue of eq. (2.6) and is shown in Fig. 2 for $m = 1$ and $k^2 = 0.5$,[25,33] is considered to be vibrations of DC lattice; the acoustic mode of the DC lattice in the first Brillouin zone and the optical mode in the extended zone.[25,33] In this classical treatment, there exists a critical wave number, π/l, which separates the region of the acoustic and optical mode. This π/l characterizes how the metallic state

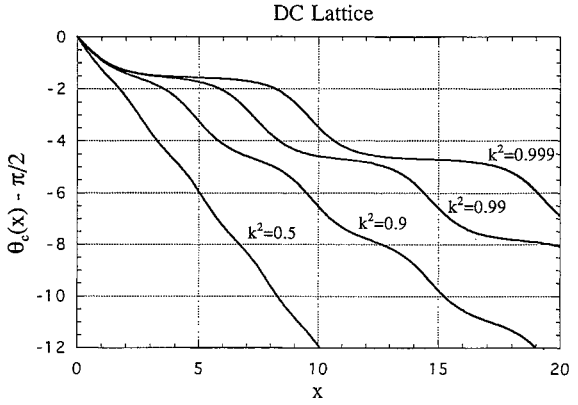

Fig. 1. The classical solution is plotted for $m = 1$ and $k^2 = 0.5$, 0.9, 0.99, 0.999.

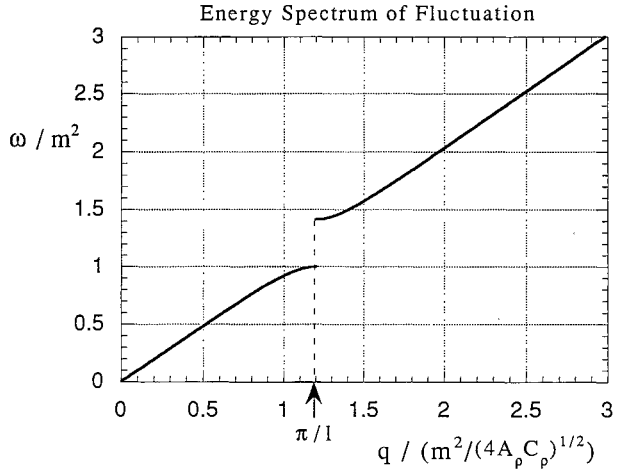

Fig. 2. Energy spectrum of the fluctuation around the classical solution is plotted for $m = 1$ and $k^2 = 0.5$.

merges into the Mott insulator. At the C-IC transition, the acoustic mode disappears and only the optical mode survives. These characteristic features are held even in fully quantum mechanical treatment, as we will see. Although general features of excitation spectrum can be understood by the classical picture, the details of this spectrum, the compressibility, and the optical conductivity should be disclosed in the quantum treatment.

2.2 *Massive Thirring model*

To solve eq. (2.1) quantum mechanically, we describe the charge degree of freedom in terms of spinless Fermion[14-16,19,20] instead of Boson. Equation (2.1) is mapped onto the following Hamiltonian (see Appendix A),

$$H_{\rho,F} = v_c \int \mathrm{d}x(\Psi^\dagger(x)(-\mathrm{i}\partial\tau_3)\Psi(x)) + \frac{v_c q_0}{2}\Psi^\dagger(x)\Psi(x) + V\int \mathrm{d}x\Psi^\dagger(x)\tau_1\Psi(x) + \frac{W}{2/\pi}\int \mathrm{d}x[(\Psi^\dagger(x)\Psi(x))^2 - (\Psi^\dagger(x)\tau_1\Psi(x))^2], \tag{2.10}$$

where

$$\Psi = \begin{pmatrix} \psi_1(x) \\ \psi_2(x) \end{pmatrix},$$
$$v_c = \pi A_\rho + C_\rho\frac{1}{\pi},$$
$$V = B_\rho(\pi\alpha),$$
$$W = \pi A_\rho - C_\rho\frac{1}{\pi},$$

and τ_j, $(j = 0, 1, 2, 3)$ are Pauli matrices. The second term, which originates from the Umklapp scattering process, creates the charge gap (Mott-Hubbard gap). This field operator, $\Psi(x)$, is identified as a charge particle because $\Psi(x)$ creates a DC in $\theta(x)$ as follows,[15,27]

$$[\theta(x), \psi_j^\dagger(y)] = \frac{\pi}{2}\mathrm{sgn}(x-y)\psi_j^\dagger(y) \qquad (j = 1, 2). \tag{2.11}$$

As mentioned in the preceding section (see eq. (2.9)), this DC corresponds to a charge particle. In the following discussion, we will set $W = 0$ and then eq. (2.10) represents a system of free Fermions. This particular choice, $W = 0$, is a good approximation near the Mott transition as has been noted by Giamarchi.[16] The reason is as follows; if $W = 0$ we see

$$A_\rho = \frac{v_\rho}{4\pi K_\rho},$$
$$C_\rho = \pi v_\rho K_\rho,$$

therefore,

$$K_\rho = \frac{1}{2}, \tag{2.12}$$

where v_ρ is the velocity of charge excitation and K_ρ is the critical exponent for the density correlation function. On the other hand, it is known that both quantities, v_ρ and K_ρ, are generally determined by the degree of the filling of band and the coupling constant. Especially, K_ρ approaches 1/2 near the half-filling for any values of coupling constant.[6-8] It is noted that K_ρ also becomes to 1/2 toward the infinite repulsive interaction for any filling as noted by Emery.[15]

2.3 *Energy spectra and compressibility*

With $W = 0$, we can solve eq. (2.10) exactly and get a simple physical picture about the charge degree of freedom near the Mott transition.[15,16,19,20] First, the energy dispersion is

$$E_-(k) = \frac{v_c q_0}{2} - \sqrt{v_c^2k^2 + V^2}, \tag{2.13}$$

$$E_+(k) = \frac{v_c q_0}{2} + \sqrt{v_c^2k^2 + V^2}. \tag{2.14}$$

The band structure relative to the chemical potential is shown schematically in Fig. 3. The actual carrier density (doped hole density) away from half-filling, δ, is determined by the range of k which satisfies $E_-(k) \geq 0$. For $q_0 > q_c \equiv 2V/v_c$, δ is determined by,

$$\delta = \frac{v_c}{2\pi V}\sqrt{q_0^2 - q_c^2}, \tag{2.15}$$

and $\delta = 0$ for $q_0 < q_c$. This relation determines the carrier density as a function of the chemical potential,

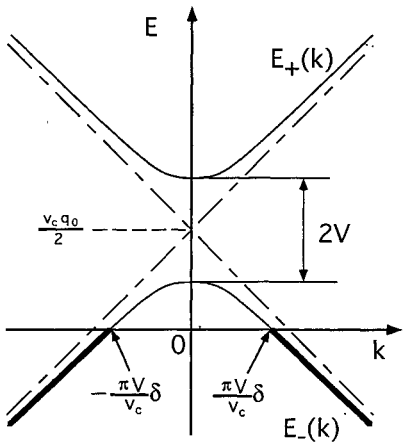

Fig. 3. The band structure of the spinless Fermion (the charge degree of freedom) for finite δ.

q_0. Consequently we immediately see that the compressibility, $\kappa = \partial n/\partial\mu$, diverges inversely proportional to the doping rate[16,20] as found in the study by Usuki, Kawakami and Okiji based on the Bethe Ansatz,[4] because of the particular energy dependence of the density of states at the band edge in one dimension.

§3. Charge Excitation and Conductivity in the Clean System

We will first calculate the density-density correlation function and next the conductivity and Drude weight by use of the Nambu formalism (see Appendix B).

3.1 Charge excitation spectrum

The charge excitation spectrum is given by the imaginary part of the retarded density-density correlation function, Im $N^R(q,\omega)$. Since we are interested in the spatially slowly varying part ($q \ll 2k_0$), the charge density is given by $n(x,t) = e\Psi^\dagger(x,t)\Psi(x,t)$. After straightforward calculation, we obtain the following result,

$$\begin{aligned}\text{Im } N^R(q,\omega) &= \frac{2e^2}{\hbar}\int\frac{\mathrm{d}k}{2\pi}\int\frac{\mathrm{d}\epsilon}{2\pi}(f(\epsilon)-f(\epsilon+\omega))\mathrm{Tr}[\tau_0\ \text{Im}\ \hat{G}^R(k+q,\epsilon+\omega)\tau_0\ \text{Im}\ \hat{G}^R(k,\epsilon)] \\ &= \frac{2e^2}{\hbar}\int\frac{\mathrm{d}k}{2\pi}\left[\left(v_kv_{k+q}+u_ku_{k+q}+\frac{V^2}{2E_kE_{k+q}}\right)\delta(\omega+E_{k+q}-E_k)\right. \\ &\quad \left.+\left(v_ku_{k+q}+u_kv_{k+q}-\frac{V^2}{2E_kE_{k+q}}\right)\delta(\omega-E_{k+q}-E_k)\right], \qquad (3.1)\end{aligned}$$

where τ_0 is the unit matrix and

$$\begin{aligned}u_k &= \frac{1}{2}\left(1+\frac{k}{E_k}\right), \\ v_k &= \frac{1}{2}\left(1-\frac{k}{E_k}\right), \\ E_k &= \sqrt{v_c^2k^2+V^2}. \qquad (3.2)\end{aligned}$$

In the last equation, the k-integration is carried out for $v_cq_0/2 < E_k < v_cq_0/2+\omega$, $f(\epsilon)$ is the Fermi distribution function and $\hat{G}(k,\mathrm{i}\epsilon)$ is Fourier transform of Green function defined as follows,

$$\hat{G}(x,\tau) = -\left\langle T_\tau\begin{pmatrix}\psi_1(x,\tau)\psi_1^\dagger(0,0) & \psi_1(x,\tau)\psi_2^\dagger(0,0)\\ \psi_2(x,\tau)\psi_1^\dagger(0,0) & \psi_2(x,\tau)\psi_2^\dagger(0,0)\end{pmatrix}\right\rangle.$$

The detailed explanation of the Green function is given in Appendix B. From eq. (3.1), we see that the charge excitation exists in the following regions;

1. Acoustic Excitation:

$$\begin{aligned}(v_cq)^2+4V^2-\omega^2 &\geq 0, \\ (v_cq)^2-\omega^2 &> 0, \\ v_cq_0-\omega \leq (v_cq)\sqrt{\frac{(v_cq)^2+4V^2-\omega^2}{(v_cq)^2-\omega^2}} &\leq v_cq_0+\omega.\end{aligned}$$

2. Optical Excitation:

$$\begin{aligned}(v_cq)^2+4V^2-\omega^2 &\leq 0, \\ (v_cq)^2-\omega^2 &< 0,\end{aligned}$$

$$\left\{v_cq_0-\omega \leq v_cq\sqrt{\frac{(v_cq)^2+4V^2-\omega^2}{(v_cq)^2-\omega^2}} \leq v_cq_0+\omega\right.$$

or

$$\left.-(v_cq_0-\omega) \geq v_cq\sqrt{\frac{(v_cq)^2+4V^2-\omega^2}{(v_cq)^2-\omega^2}} \geq -(v_cq_0+\omega)\right\}.$$

These regions are plotted for several choices of doping rate in Fig. 4 and actual magnitude of the spectral weight, Im $N^R(q,\omega)$, in these regions are shown in Fig. 5.[20] The existence of the acoustic mode of excitation spectrum has also been obtained from a quantum Monte Carlo simulation using the maximum entropy method for the 1D Hubbard model away from half-filling.[34] In the metallic state (far away from half-filling), the acoustic mode, which corresponds to the charge excitation in the Tomonaga-Luttinger liquid, dominates spectral weight especially around the small wave numbers. Thus it is reasonable to consider that the inter-band excitation across the Mott-Hubbard gap does not contribute to the density-density correlation function in the limit of long wave length. Near the Mott transition, however, such region where the acoustic mode is dominant becomes small and the optical mode is dominant elsewhere. This implies that, in the real space, the density-density correlation function has a characteristic length scale for the crossover behavior. The similar crossover behavior is numerically found in the spin-spin correlation function.[35] As the Mott insulator is approached, the characteristic length scale becomes large, above which

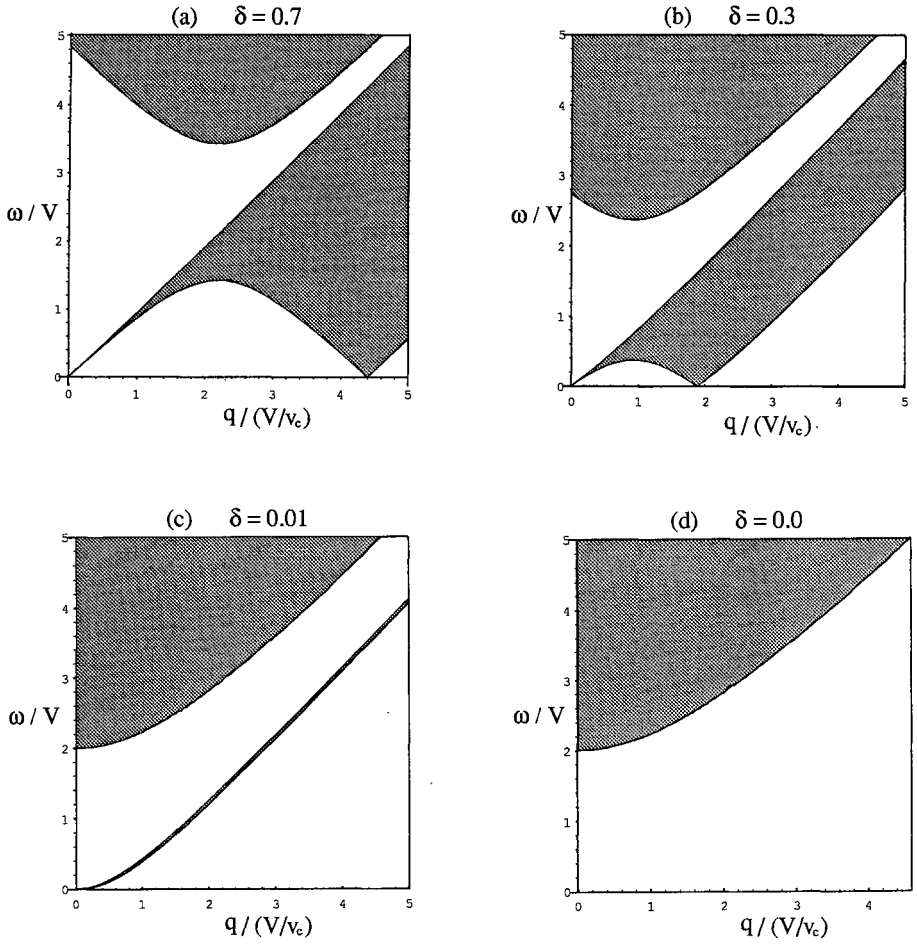

Fig. 4. The region of (q, ω) with a finite Im $N(q, \omega)$ for several choices of (a) $\delta = 0.7$, (b) $\delta = 0.3$, (c) $\delta = 0.01$, (d) $\delta = 0.0$ per one site.

the correlation function follows its asymptotic form derived by the conformal field theory. In the limit of Mott insulator, this length scale diverges and the conformal field theory breaks down. Correspondingly, the spectral weight shifts from the acoustic mode to the optical mode and the metallic phase crossover to the insulator phase. The Mott transition is characterized by this crossover,[20] which has not been so far found out by any theories. The location in q-space of this crossover about the dominant spectral weight corresponds to that of the excitation spectrum in the classical approximation as shown in Fig. 2.

3.2 *Conductivity and Drude weight*

Next the conductivity[16-18] and Drude weight[16,19,20] will be calculated by the imaginary part of retarded current-current correlation function, Im $K^R(\omega)$, which is evaluated as follows. By noting that the current density is $j(x,t) = ev_c\Psi^\dagger(x,t)\tau_3\Psi(x,t)$ because of the continuity equation, we obtain

$$\begin{aligned}\lim_{q\to 0} \text{Im } K^R(q,\omega) &= \frac{2e^2v_c^2}{\hbar}\int\frac{\mathrm{d}k}{2\pi}\int\frac{\mathrm{d}\epsilon}{2\pi}(f(\epsilon)-f(\epsilon+\omega))\lim_{q\to 0}\text{Tr}[\text{Im }\hat{G}^R(k+q,\epsilon+\omega)\tau_3\ \text{Im }\hat{G}^R(k,\epsilon)\tau_3] \\ &= \frac{2e^2v_c^2}{\hbar}\int\frac{\mathrm{d}k}{2\pi}\lim_{q\to 0}\left[\left(v_kv_{k+q}+u_ku_{k+q}-\frac{V^2}{2E_kE_{k+q}}\right)\delta(\omega+E_{k+q}-E_k)\right. \\ &\quad \left.+\left(v_ku_{k+q}+u_kv_{k+q}+\frac{V^2}{2E_kE_{k+q}}\right)\delta(\omega-E_{k+q}-E_k)\right]. \end{aligned} \tag{3.3}$$

In the last equation, the k-integration is carried out for $v_cq_0/2 < E_k < v_cq_0/2+\omega$. Near the Mott transition, the Drude weight, D_c, which is defined as, Re $\sigma(\omega) = D_c\delta(\omega)$, is calculated as follows (see also Appendix C),

$$\text{Re }\sigma(\omega) = \text{Re}\,\frac{K^R(\omega)-2v_ce^2/h}{\mathrm{i}\omega-\eta}, \tag{3.4}$$

therefore,

$$\begin{aligned} D_c &= \frac{e^2v_c}{\hbar}\frac{\delta}{q_0/2}, \\ &\sim \frac{e^2v_c}{\hbar}\frac{\delta}{V}. \end{aligned} \tag{3.5}$$

This fact, that D_c is proportional to the concentration

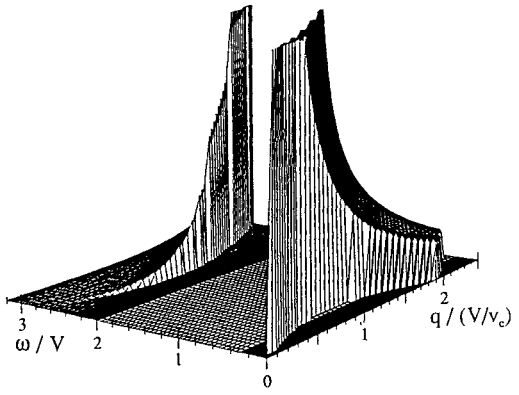

(a) ImN(q,ω) for δ = 0.3

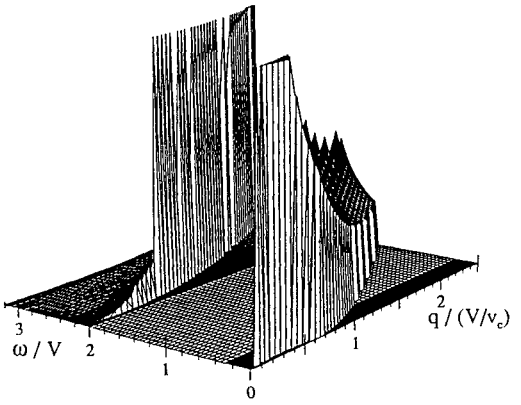

(b) ImN(q,ω) for δ = 0.1

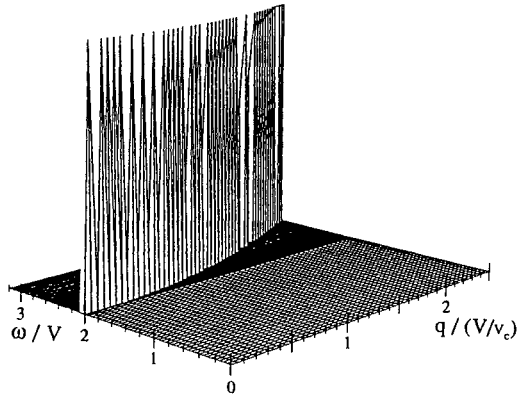

(c) ImN(q,ω) for δ = 0.0

Fig. 5. The spectral density of the charge excitations, Im $N(q,\omega)$, in the plane of q and ω for (a) $\delta = 0.3$, (b) $\delta = 0.1$, (c) $\delta = 0.0$ per one site.

of the doped holes near the Mott transition, is consistent with the exact result obtained by Shastry and Sutherland by use of the Bethe Ansatz[5] and has also been noted by Giamarchi[16] and Emery.[19] It is interesting to notice that the doping dependence of D_c is different from that of Tomonaga-Luttinger liquid. In the Tomonaga-Luttinger regime, the D_c is determined as, $2e^2 v_c/\hbar$, by the electron (particle) number density which is expressed through v_c.[13] This result is obtained by the Kubo formula by using the anomalous commutation relation which is inherent to the one dimensional systems with linear dispersion.[36] The different dependence on the carrier concentration of D_c between in the Tomonaga-Luttinger regime and near the Mott insulator results from the roles played by the Umklapp scattering process. Thus we can understand that the Umklapp scattering process plays crucial roles near the Mott transition.

§4. Impurity Effect

So far we confined ourselves to the clean system. We will in the following consider the effects of disorder represented by the impurity scattering. We first explain how to introduce and treat impurity scattering, and then we study the effects of impurity scattering on the density of states, which determines the compressibility and the conductivity. We will employ the self-consistent Born approximation and ignore the possible consequence of the Anderson localization or the bound states in the Mott-Hubbard gap in order to understand overall features in the present study.

4.1 Impurity Hamiltonian and self-energy

The impurity potential, $u(x)$, couples to the charge density, $\rho(x)$, as follows,

$$H_{\rm imp} = \sum_i \int {\rm d}x u(x - R_i)\rho(x) \tag{4.1}$$

where $\rho(x)$ is expressed as follows,

$$\rho(x) = \psi_1^\dagger(x)\psi_1(x) + \psi_2^\dagger(x)\psi_2(x) + {\rm e}^{-{\rm i}\lambda x}\psi_1^\dagger(x)\psi_2(x) + {\rm e}^{{\rm i}\lambda x}\psi_2^\dagger(x)\psi_1(x). \tag{4.2}$$

The oscillating part of $\rho(x)$, which is characterized by the constant, λ, originates in the density fluctuation across the Fermi surface of spinless fermion. We suppose the impurity potential to be the δ-function, $u(x) = u\delta(x)$. In this impurity scattering Hamiltonian, we ignored the coupling between the charge and spin excitation through the $2k_{\rm F}$-oscillating part of charge density.[37]

In the second order self-consistent Born approximation, the self-energy, which is diagrammatically shown in the Fig. 6, is given as follows;

$$\hat{\Sigma}(z) = \begin{pmatrix} \sigma(z) & \Delta^\dagger(z) \\ \Delta(z) & \sigma(z) \end{pmatrix} = n_i u^2 \int \frac{{\rm d}k}{2\pi} \begin{pmatrix} g_1(k,z) + g_2(k,z) & f^\dagger(k,z) \\ f(k,z) & g_1(k,z) + g_2(k,z) \end{pmatrix}, \tag{4.3}$$

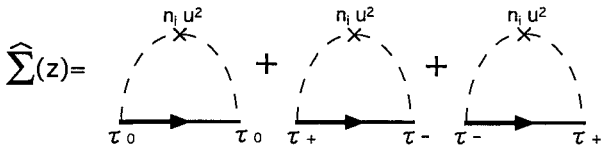

Fig. 6. The Feynman diagram for the self-energy. The thick line means the full Green function and the broken line represent the impurity scattering.

where

$$\sigma(z) = -\mathrm{i}\frac{n_i u^2}{v_c}\frac{\tilde{z}}{\sqrt{\tilde{z}^2 - \tilde{V}^2}}$$

$$\Delta(z) = \Delta^{\dagger}(z) = -\mathrm{i}\frac{n_i u^2}{2v_c}\frac{\tilde{V}}{\sqrt{\tilde{z}^2 - \tilde{V}^2}}, \qquad (4.4)$$

which are easily obtained after k-integration. For details of $\tilde{z}, \tilde{V}$, see Appendix B. The self-consistent equations eqs. (4.3) and (4.4) are reduced to the following equations,

$$\tilde{z} = z - \sigma(z) = z + \mathrm{i}\frac{n_i u^2}{v_c}\frac{\tilde{z}}{\sqrt{\tilde{z}^2 - \tilde{V}^2}},$$

$$\tilde{V} = V + \Delta(z) = V - \mathrm{i}\frac{n_i u^2}{2v_c}\frac{\tilde{V}}{\sqrt{\tilde{z}^2 - \tilde{V}^2}}. \qquad (4.5)$$

Equation (4.5) is rewritten as

$$\chi^4 - 2y\chi^3 + (y^2 + \zeta^2 - 1)\chi^2 + 2y\chi - y^2 = 0 \qquad (4.6)$$

where $\zeta = 3n_i u^2/2v_c V$, $\chi = \tilde{z}/\tilde{V}$ and $y = z/V$.

4.2 Density of states and compressibility

By using the solution of eq. (4.6), the density of states, $\mathcal{D}(\epsilon)$, is calculated as follows,

$$\mathcal{D}(\epsilon) = -\frac{1}{\pi}\int\frac{\mathrm{d}k}{2\pi}\,\mathrm{Im\ Tr}\,[\hat{G}^R(k,z)],$$

$$= \frac{1}{\pi v_c}\,\mathrm{Re}\,\frac{\chi}{\sqrt{\chi^2 - 1}},$$

$$= \frac{1}{\pi v_c \zeta}\,\mathrm{Im}\,(\chi). \qquad (4.7)$$

$\mathcal{D}(\epsilon)$ is plotted in Fig. 7 for several choices of dimensionless parameter, ζ, representing the strength of impurity scattering. It should be noted that, in the presence of impurity scattering, the Mott-Hubbard gap, which is considered to be the energy gap in the density of states of spinless Fermion, exists for $0 < \zeta < 1$. In the following, we will use the term 'weak disordered system' to refer to the system for $0 < \zeta < 1$. On the other hand, for $\zeta \geq 1$, the gap disappears but the density of states has a cusp at $\epsilon = 0$.

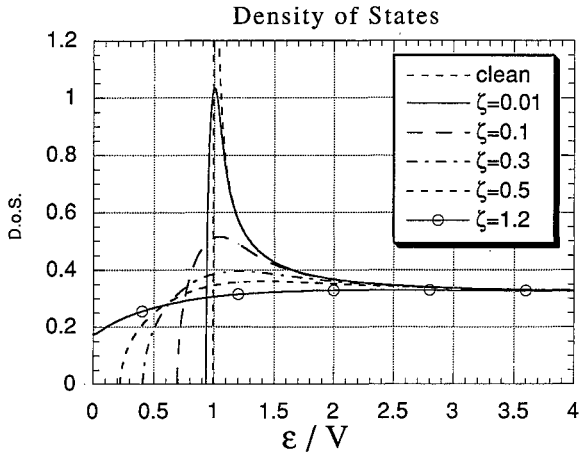

Fig. 7. The density of states is plotted for $\zeta = 0$, 0.01, 0.1, 0.3, 0.5, 1.2.

In addition to the change of Mott-Hubbard gap, the $\mathcal{D}(\epsilon)$ in the disordered systems does not diverge at the band edge in contrast to the $\mathcal{D}(\epsilon)$ in the clean system. This qualitative change of density of states directly affects the compressibility, $\kappa = \partial n/\partial\mu$; In the clean system κ diverges, but in the weak disordered system, it smoothly vanishes as $\delta^{2/3}$ as is shown in Fig. 8. Though the value of the critical exponent 2/3 should not be taken literally in view of the approximation employed, this drastic qualitative difference between the clean and disordered systems is to be noted. For $\zeta \geq 1$, κ approaches a finite constant.

4.3 Charge excitation spectrum in the disordered system

In the calculation of the density-density correlation function, $N(q,\omega)$, we need the vertex correction in addition to the self-energy correction. The vertex corrections to the density vertex, $\hat{\Gamma}_N(q,\omega)$, is the solution of following Dyson equation,

$$\hat{\Gamma}_N(q,\mathrm{i}\omega) = \tau_0 + \frac{2\zeta}{3V}\int\frac{\mathrm{d}k}{2\pi}\Big[\hat{G}(k+q,z+\mathrm{i}\omega)\tau_0\hat{G}(k,z) + \tau^+\hat{G}(k+q,z+\mathrm{i}\omega)\tau_0\hat{G}(k,z)\tau^-$$
$$+ \tau^-\hat{G}(k+q,z+\mathrm{i}\omega)\tau_0\hat{G}(k,z)\tau^+ + \hat{G}(k+q,z+\mathrm{i}\omega)\hat{\Gamma}_N(q,\mathrm{i}\omega)\hat{G}(k,z)$$
$$+ \tau^+\hat{G}(k+q,z+\mathrm{i}\omega)\hat{\Gamma}_N(q,\mathrm{i}\omega)\hat{G}(k,z)\tau^- + \tau^-\hat{G}(k+q,z+\mathrm{i}\omega)\hat{\Gamma}_N(q,\mathrm{i}\omega)\hat{G}(k,z)\tau^+\Big], \qquad (4.8)$$

where $\tau^{\pm} = (\tau_1 \pm \mathrm{i}\tau_2)/2$ and τ_0 is the unit matrix. $N(q,\mathrm{i}\omega)$ is calculated by using the solution of the above equation as follows,

$$N(q,\mathrm{i}\omega) = \frac{\mathrm{e}^2}{h}(-T)\sum_z\int\frac{\mathrm{d}k}{2\pi}\mathrm{Tr}\left[\tau_0\hat{G}(k+q,z+\mathrm{i}\omega)\hat{\Gamma}_N(q,\mathrm{i}\omega)\hat{G}(k,z)\right]. \qquad (4.9)$$

Im $N(q,\omega)$ are plotted in Fig. 9 for several values of δ, ζ and q, by solving the above equation numerically. In the weak disordered systems, there also exist the acoustic excitation and the optical excitation as in the clean system, though these excitations are damped. Hence, the crossover feature of spectral weight in q and ω-space

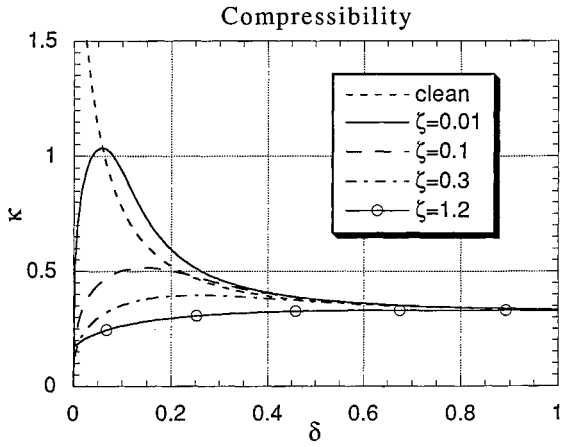

Fig. 8. The compressibility is plotted for $\zeta = 0$, 0.01, 0.1, 0.3, 0.5.

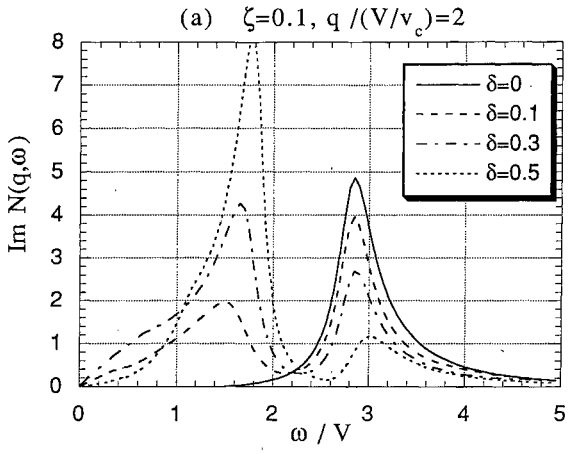

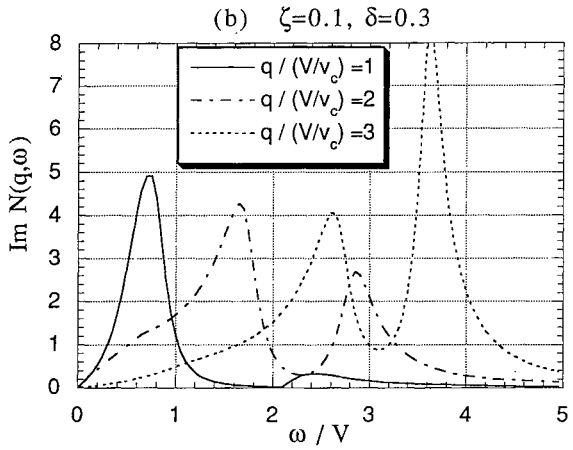

Fig. 9. The spectral density of the charge excitations, Im $N(q,\omega)$, in the disordered system as the function of ω for (a) $\delta = 0.0$, 0.1, 0.3, 0.5, $q = 2$ and (b) $q = 1$, 2, 3, $\delta = 0.3$.

survives as far as the impurity scattering is not so strong as seen in Fig. 9 for $\zeta = 0.1$ and $\delta = 0.3$. The doping dependence of spectral weight is shown in Fig. 9 for $\zeta = 0.1$ and $q = 2$, where it is seen that the dominant excitation smoothly changes from the acoustic (optical) excitation to the optical (acoustic) excitation as the doping rate is varied. Therefore the crossover behavior in the vicinity of the Mott transition is visible not only in the clean system but is present also in the weak disordered systems as well.

4.4 Optical conductivity and Drude weight in the disordered system

In the calculation of the conductivity, we need the vertex correction for the current vertex, $\hat{\Gamma}_K(0,\omega)$, again similar to that of density-density correlation function; i.e., insert τ_3 between Green functions for the first, second and third term in eq. (4.8) and take the limit of $q \to 0$.

$$\begin{aligned}\hat{\Gamma}_K(\mathrm{i}\omega) = \tau_3 + \frac{2\zeta}{3V}\int\frac{\mathrm{d}k}{2\pi}\Big[&\hat{G}(k,z+\mathrm{i}\omega)\tau_3\hat{G}(k,z) + \tau^+\hat{G}(k,z+\mathrm{i}\omega)\tau_3\hat{G}(k,z)\tau^- \\ &+ \tau^-\hat{G}(k,z+\mathrm{i}\omega)\tau_3\hat{G}(k,z)\tau^+ + \hat{G}(k+q,z+\mathrm{i}\omega)\hat{\Gamma}_K(\mathrm{i}\omega)\hat{G}(k,z) \\ &+ \tau^+\hat{G}(k+q,z+\mathrm{i}\omega)\hat{\Gamma}_K(\mathrm{i}\omega)\hat{G}(k,z)\tau^- + \tau^-\hat{G}(k,z+\mathrm{i}\omega)\hat{\Gamma}_K(\mathrm{i}\omega)\hat{G}(k,z)\tau^+\Big]. \qquad (4.10)\end{aligned}$$

The current-current correlation function, $K(\mathrm{i}\omega)$, with vertex correction is calculated as follows,

$$K(\mathrm{i}\omega) = \frac{(\mathrm{e}v_c)^2}{h}(-T)\sum_z\int\frac{\mathrm{d}k}{2\pi}\mathrm{Tr}\left[\tau_3\hat{G}(k,z+\mathrm{i}\omega)\hat{\Gamma}_K(\mathrm{i}\omega)\hat{G}(k,z)\right]. \qquad (4.11)$$

The optical conductivity is obtained by solving the above equation numerically. In Fig. 10, the ω-dependence of optical conductivity in the case of $\delta = 0.01$ is shown for several choices of $\zeta = 0.0$, 0.01, 0.1, 0.3. There exist optical absorption across the Mott-Hubbard gap as well as the Drude tail. Because of the impurity scattering, both spectra become broad and difficult to distinguish from each another if the impurity scattering becomes strong. An example of the doping dependence of the optical conductivity in the weak disordered systems is plotted for $\zeta = 0.1$ and some choices of δ in Fig. 11. In this figure, the Drude weight seems to behave similarly to that of clean system as a function of doping rate, i.e., smoothly approaches to zero. It becomes clear by comparing the integrated weight of both, Drude and optical, that the missing weight of Drude peak shifts to the optical absorption and the metallic state merges to the insulator phase. These general features of optical conductivity is plausible but it has not been explicitly demonstrated so far. The crossover feature near the Mott transition appears as the smooth shift of weight in the optical conductivity.

§5. Conclusion and Discussion

In the present study, we investigated the excitation

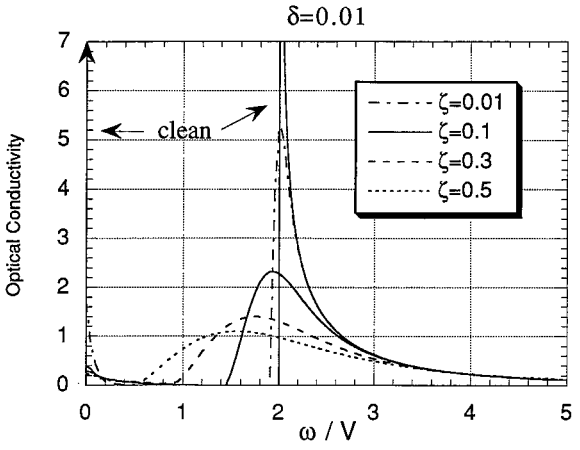

Fig. 10. The optical-conductivity is plotted for $\delta = 0.01$, and $\zeta = 0.0, 0.01, 0.1, 0.3, 0.5$.

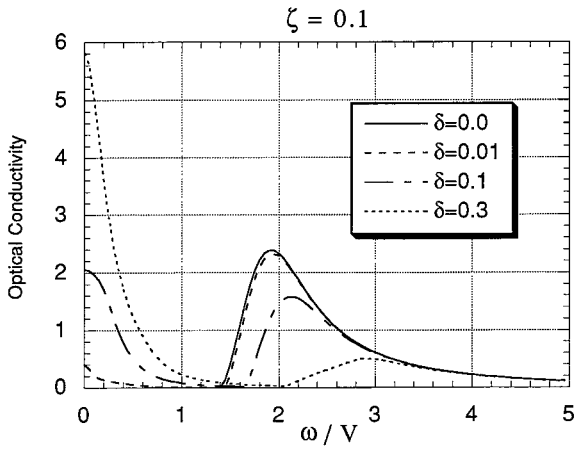

Fig. 11. The optical-conductivity is plotted for $\zeta = 0.1$, and $\delta = 0.0, 0.01, 0.1, 0.3$.

spectrum of density-density correlation function and the optical conductivity near the Mott transition in one-dimensional electron system in the presence of disorder. Those quantities were calculated based on the massive Thirring model for the spinless Fermion. In the Mott insulator, i.e., at half-filling, the Mott-Hubbard gap was seen to originate from the Umklapp scattering process as noted by Emery.[14,15,19] Even in the doped Mott insulator, i.e., away from half-filling, this process played the important role as indicated by Giamarchi.[16] First, we calculated the static limit of the density-density correlation function and the conductivity, i.e., compressibility[16,20] and Drude weight.[16,19,20] In the clean system, the doping dependence of both quantities were same as the results deduced by the exact solution.[4] Although the Drude weight did not qualitatively change its behavior also in the weak disordered systems, the compressibility even in the weak disordered systems behaved completely different way from that in the clean system. Next, we studied the dynamical properties. In both the clean and weak disordered systems, the crossover behavior existed in the spectra of density-density correlation function; in the region of small wave number, the acoustic mode was dominant while in the large wave number region, the optical mode was weighted. By decreasing the doping rate, the region, in which the acoustic mode was dominant, became small and its spectral weight shifted to that of optical mode. We would like to emphasize that the Mott transition was characterized by the crossover feature rather than drastic phase transition. The smooth shift of spectral weight from the Drude weight to the optical absorption is present in the optical conductivity in both the clean and weak disordered systems. If the impurity scattering becomes strong and the effect of localization becomes important,[38] the optical conductivity would vanish as approaching $\omega = 0$ and will show an characteristic features of the pinning frequency.[39]

Acknowledgements

M. M. would like to thank Hiroshi Kohno and Hideaki Maebashi for their valuable discussions. Thanks are due to Professor T. Giamarchi and Professor V. J. Emery for valuable comments. This work was financially supported by a Grant-in-Aid for Scientific Research on Priority Area "Anomalous Metallic State near the Mott Transition" (07237102) from the Ministry of Education, Science, Sports and Culture.

Appendix A: Mapping from Phase Hamiltonian to Massive Thirring Model

The equivalence between the two Hamiltonians eqs. (2.1) and (2.10) is proved by the bosonization method. To begin with, we define the boson operators, $\theta_j(x)$ $(j = 1, 2)$, in terms of the spinless Fermions $\psi_j(x)$ $(j = 1, 2)$ as follows,

$$\theta(x) \equiv \frac{1}{2}(\theta_1(x) + \theta_2(x)), \tag{A·1}$$

$$\theta_j \equiv \mathrm{i}\sum_q \frac{2\pi}{Lq} \exp(-\mathrm{i}qx - \frac{1}{2}\alpha|q|)\rho_j(q), \ (j = 1, 2), \tag{A·2}$$

$$\rho_j(q) \equiv \sum_k c^\dagger_{j,k+q} c_{j,k}, \ (q > 0),$$

$$\rho_j(-q) \equiv \sum_k c^\dagger_{j,k} c_{j,k+q}, \ (q > 0), \tag{A·3}$$

where

$$[\rho_1(-q), \rho_1(q')] = [\rho_2(q), \rho_2(-q')] = \frac{Lq}{2\pi}\delta_{q,q'}. \tag{A·4}$$

The spinless Fermions correspond to those Boson operators as follows,

$$\psi_i(x) = \frac{1}{\sqrt{2\pi\alpha}} \exp(\pm\mathrm{i}\theta_i(x)), \ (+ \text{ for } i = 1, - \text{ for } i = 2). \tag{A·5}$$

The Hamiltonian eq. (2.1) is described in terms of the density operators as follows,

$$\int \mathrm{d}x(\nabla\theta(x))^2 = \pi \int_{q>0} \mathrm{d}q \left[\rho_1(q)\rho_1(-q) + \rho_2(-q)\rho_2(q) + \rho_1(q)\rho_2(-q) + \rho_1(-q)\rho_2(q)\right],$$

$$\int \mathrm{d}x(P(x))^2 = \frac{1}{\pi}\int_{q>0} \mathrm{d}q\,[\rho_1(q)\rho_1(-q) + \rho_2(-q)\rho_2(q) - \rho_1(q)\rho_2(-q) - \rho_1(-q)\rho_2(q)],$$

thus,

$$A_\rho \int \mathrm{d}x(\nabla\theta(x))^2 + C_\rho \int \mathrm{d}x(P(x))^2 = \left(\pi A_\rho + \frac{C_\rho}{\pi}\right)\int_{q>0} \mathrm{d}q\,[\rho_1(q)\rho_1(-q) + \rho_2(-q)\rho_2(q)] + \left(\pi A_\rho - \frac{C_\rho}{\pi}\right)\int_{q>0} \mathrm{d}q\,[\rho_1(q)\rho_2(-q) + \rho_1(-q)\rho_2(q)]. \quad \text{(A·6)}$$

Next, the first and third term of eq. (2.10) are also written in terms of the density operators as follows,

$$H^{(1)}_{\rho,D} = v_c \int_{q>0} \mathrm{d}q\,[\rho_1(q)\rho_1(-q) + \rho_2(-q)\rho_2(q)],$$
$$H^{(3)}_{\rho,D} = W \int_{q>0} \mathrm{d}q\,[\rho_1(q)\rho_2(-q) + \rho_1(-q)\rho_2(q)] \quad \text{(A·7)}$$

which are proved by the following equations, *e.g.*,

$$\left[H^{(1)}_{\rho,F}, \rho_{1,\sigma}(q)\right] = v_c q \rho_{1,\sigma}(q), \quad \text{(A·8a)}$$
$$\left[H^{(1)}_{\rho,D}, \rho_{1,\sigma}(q)\right] = v_c q \rho_{1,\sigma}(q), \quad \text{(A·8b)}$$

for the first term of eq. (2.10). By comparing eqs. (A·6) and (A·7), we see the following relations,

$$v_c = \pi A_\rho + C_\rho \frac{1}{\pi},$$
$$W = \pi A_\rho - C_\rho \frac{1}{\pi},$$

B_ρ term is easily derived by inserting eq. (A·5) into the second term of eq. (2.10).

Appendix B: Definition of Green Function

In the Nambu formalism for the charge degree of freedom near the Mott transition, the Green function, $\hat{G}(x,\tau)$, is defined as 2×2 matrix,

$$\hat{G}(x,\tau) = -\left\langle T_\tau \begin{pmatrix} \psi_1(x,\tau)\psi_1^\dagger(0,0) & \psi_1(x,\tau)\psi_2^\dagger(0,0) \\ \psi_2(x,\tau)\psi_1^\dagger(0,0) & \psi_2(x,\tau)\psi_2^\dagger(0,0) \end{pmatrix}\right\rangle, \quad \text{(B·1)}$$

where T_τ means the chronological order in the imaginary time. In the clean system, after Fourier transformation for the system without the interaction, $W = 0$,

$$\hat{G}^0(k,z) = \begin{pmatrix} g_1^0(k,z) & f^{\dagger,0}(k,z) \\ f^0(k,z) & g_2^0(k,z) \end{pmatrix} = \begin{pmatrix} z - v_c k & -V \\ -V & z + v_c k \end{pmatrix}^{-1}, \quad \text{(B·2)}$$

where $z = \mathrm{i}\epsilon - v_c q_0/2$.

In the disordered systems, full Green function, $\hat{\boldsymbol{G}}(k,z)$, including the self-energy correction is calculated as follows,

$$\hat{\boldsymbol{G}}(k,z) = \left(\hat{G}^0(k,z)^{-1} - \hat{\Sigma}(z)\right)^{-1} = \begin{pmatrix} z - v_c k - \sigma(z) & -V - \Delta^\dagger(z) \\ -V - \Delta(z) & z + v_c k - \sigma(z) \end{pmatrix}^{-1}. \quad \text{(B·3)}$$

We take the full Green function as follows to determine the self-energy (or Green function),

$$\hat{\boldsymbol{G}}(k,z) = \begin{pmatrix} \boldsymbol{g}_1(k,z) & \boldsymbol{f}^\dagger(k,z) \\ \boldsymbol{f}(k,z) & \boldsymbol{g}_2(k,z) \end{pmatrix} = \begin{pmatrix} \tilde{z} - v_c k & -\tilde{V}^\dagger \\ -\tilde{V} & \tilde{z} + v_c k \end{pmatrix}^{-1}. \quad \text{(B·4)}$$

We can derive the self-consistent equation eq. (4.5) by substituting eq. (B·4) to eq. (4.3).

Appendix C: Calculation of Drude Weight near the Mott Transition

An uniform electric field, $E_x(t)$, along the one dimensional system has such a relation, $E_x(t) = \partial_x A_0(x,t) - \partial_t A_1(x,t)$, to the vector potential, $\boldsymbol{A}(x,t) = (A_0(x,t), A_1(x,t))$. To make our discussion simple, we introduce external field as follows, $\boldsymbol{A}(x,t) = (xE_x(t), 0)$. The perturbation term by the external field, $\mathcal{H}_{\mathrm{ext}}$, is introduced as ordinary way,

$$\mathcal{H}_{\mathrm{ext}} = -e\int \mathrm{d}x n(x) A_0(x,t). \quad \text{(C·1)}$$

On these grounds, the conductivity, $\sigma(\omega)$, is calculated as follows,

$$\sigma(\omega) = \frac{\mathrm{i}}{\hbar} e \int_0^\infty \mathrm{d}s \int_{-\infty}^\infty \mathrm{d}y \mathrm{e}^{\mathrm{i}\omega s}\langle[J(s), n(0,y)]\rangle y, = \frac{\mathrm{i}}{\hbar} e \int_{-\infty}^\infty \mathrm{d}y \frac{-1}{\mathrm{i}\omega - \eta}\langle[J(0), n(0,y)]\rangle y + \frac{\mathrm{i}}{\hbar}\int_0^\infty \mathrm{d}s \frac{\mathrm{e}^{(\mathrm{i}\omega-\eta)s}}{\mathrm{i}\omega-\eta}\int_{-\infty}^\infty \mathrm{d}y\langle[J(0), j(-s,y)]\rangle. \quad \text{(C·2)}$$

where the translational invariance in space coordinate and the continuity equation are noted.
In eq. (C·2), the first term in the last equation is estimated as,

$$\frac{\mathrm{i}}{\hbar}\int_{-\infty}^\infty \mathrm{d}y \frac{-1}{\mathrm{i}\omega-\eta}\langle[J(0), n(0,y)]\rangle y = \frac{2e^2 v_c}{h}\frac{-1}{\mathrm{i}\omega-\eta}, \quad \text{(C·3)}$$

by using the anomalous commutation relation,

$$[j(x), n(y)] = \frac{\mathrm{i}e v_c}{\pi}\partial_x \delta(x-y). \quad \text{(C·4)}$$

As a result, the real part of conductivity is calculated as follows,

$$\mathrm{Re}\,\sigma(\omega) = \mathrm{Re}\,\frac{K^R(\omega) - 2v_c e^2/h}{\mathrm{i}\omega - \eta}, = \left\{\mathrm{Re}\,K^R(\omega) - \frac{2v_c e^2}{h}\right\}(-\pi)\delta(\omega) + \frac{\mathrm{Im}\,K^R(\omega)}{\omega}. \quad \text{(C·5)}$$

Without the Umklapp scattering process in the last equation, the terms corresponding to the $K^R(\omega)$ is zero and the Drude weight takes the constant value, $2e^2v_c/h$.

1) J. Hubbard: Proc. R. Soc. London, Ser. A **281** (1964) 401.
2) W. F. Brinkman and T. M. Rice: Phys. Rev. B **2** (1970) 4302.
3) E. H. Lieb and F. Y. Wu: Phys. Rev. Lett. **20** (1968) 1445.
4) T. Usuki, N. Kawakami and A. Okiji: Phys. Lett. **135A** (1989) 476.
5) B. S. Shastry and B. Sutherland: Phys. Rev. Lett. **65** (1990) 243.
6) N. Kawakami and S. K. Yang: Phys. Lett. **148A** (1990) 359.
7) H. Frahm and V. E. Korepin: Phys. Rev. B **42** (1990) 10553.
8) H. Schulz: Phys. Rev. Lett. **64** (1990) 2831.
9) S. Tomonaga: Prog. Theor. Phys. **5** (1950) 349.
10) J. M. Luttinger: Phys. Rev. **4** (1963) 1154.
11) V. J. Emery: *Highly Conducting One-Dimensional Solids*, ed. J. Devreese, R. Evrad and V. van Doren (Plenum, New York, 1979) p. 247.
12) J. Solyom: Adv. Phys. **28** (1979) 201.
13) H. Fukuyama and H. Takayama: *Electronic Properties of Inorganic Quasi-One-Dimensional Compounds Part 1*, ed. P. Monceau (D. Reidel Pub. Co., Dordrecht, 1985) p. 41.
14) V. J. Emery, A. Luther and I. Peschel: Phys. Rev. B **13** (1976) 1272.
15) V. J. Emery: Phys. Rev. Lett. **65** (1990) 1076.
16) T. Giamarchi: Phys. Rev. B **44** (1991) 2905.
17) T. Giamarchi: Phys. Rev. B **46** (1992) 342.
18) T. Giamarchi and A. J. Millis: Phys. Rev. B **46** (1991) 9325.
19) V. J. Emery: *Correlated Electron Systems*, ed. V. J. Emery (World Scientific, Singapore, 1993) Vol. 9, p. 166.
20) M. Mori, H. Fukuyama and M. Imada: J. Phys. Soc. Jpn. **63** (1994) 1639.
21) Y. Suzumura: Prog. Theor. Phys. **61** (1979) 1.
22) V. J. Emery: *Proceedings of Kyoto Summer Institute 1979 - Physics of Low-Dimensional Systems*, ed. Y. Nagaoka and S. Hikami (Publication Office, Progress of Theoretical Physics, 1979).
23) F. D. M. Haldane: Phys. C **14** (1981) 2585; Phys. Rev. Lett. **47** (1981) 1840.
24) K. Penc and J. Solyom: Phys. Rev. B **47** (1993) 6273.
25) W. L. McMillan: Phys. Rev. B **14** (1976) 1496; *ibid.* B **16** (1977) 4655.
26) S. Coleman: Phys. Rev. D **11** (1975) 2088.
27) S. Mandelstam: Phys. Rev. D **11** (1975) 3026.
28) Y. Okwamoto: J. Phys. Soc. Jpn. **49** (1980) 8.
29) S. Takada and S. Misawa: Prog. Theor. Phys. **66** (1981) 101.
30) K. Hida, M. Imada and M. Ishikawa: J. Phys. C **16** (1983) 4945.
31) A. Luther and V. J. Emery: Phys. Rev. Lett. **33** (1974) 589.
32) P. A. Lee: Phys. Rev. Lett. **34** (1975) 1247.
33) B. Sutherland: Phys. Rev. A **8** (1973) 2514.
34) R. Preuss, A. Muramatsu, W. von der Lindon, F. F. Assaad and W. Hanke: Phys. Rev. Lett. **73** (1994) 732.
35) M. Imada, N. Furukawa and T. M. Rice: J. Phys. Soc. Jpn. **61** (1992) 3861.
36) F. D. M. Haldane: Phys. Rev. Lett. **74** (1995) 2090.
37) Y. Suzumura, T. Saso, H. Fukuyama and J. L. Cardy: *Proc. Int. Conf. LT-17, Karlsruche, 1984* (Elsevier Science, Amsterdam, 1984) p. 891.
38) Y. Suzumura and H. Fukuyama: J. Phys. Soc. Jpn. **53** (1984) 3918.
39) H. Fukuyama and P. A. Lee: Phys. Rev. B **17** (1978) 535.

Noto added in proof—S. Fujimoto and N. Kawakami (Phys. Rev. B **54** (1996) 11018R) also investigated the disorder effect on the Mott insulator, i.e. at half-filling, by use of replica trick and renormalization group method. They concluded that for sufficient large values of the forward scattering by impurities the Umklapp scattering process became irrelevant and the gap in the charge excitation disappeared whereas the backward scattering by impurities drove the system to the Anderson localized state.